



# Neutron beam characterization for the Moroccan TRIGA Mark II reactor

Hamid Amsil<sup>1,2</sup> · Abdelhamid Jalil<sup>2</sup> · Oudie Kabach<sup>2</sup> · Hassan Chahidi<sup>3</sup> · Hamid Bounouira<sup>1</sup> · Chafik Elyounoussi<sup>1</sup> · Abdelouahed Chetaine<sup>2</sup>

Received: 20 June 2020 / Accepted: 19 January 2021 / Published online: 5 February 2021  
© Akadémiai Kiadó, Budapest, Hungary 2021

## Abstract

The TRIGA Mark II research reactor is equipped with four horizontal beam tubes and one thermal column. The tangential (NB1) and Percy (NB2) beam tube, which are the subject of this study, are dedicated to Prompt Gamma Neutron Activation Analysis and Neutron Imaging, and (Neutron Diffraction) facilities, respectively. A preliminary neutron characterization is needed for each beam tube. Basic beam parameters, including neutron flux, were measured with threshold activation detectors for the two beam tubes (NB1, NB2). Activity measurement through gamma spectrometry was performed with a high-purity germanium detector to evaluate the neutron flux through multiple analyses of activation detectors. The results were compared with those obtained using an approximated Monte Carlo simulation model for the reactor. A comparison between the experimental and simulated results revealed a good level of agreement.

**Keywords** Neutron flux · Neutron beam · Activation detectors · MCNP6

**Mathematics Subject Classification** 00-01 · 99-00

## Introduction

The TRIGA Mark II research reactor (TMIIRR) is located at the National Centre for Nuclear Energy, Sciences and Technology (CNESTEN), Morocco. Its purpose is to contribute to the development of various socio-economic sectors in the country, such as the environment and geochemistry, agriculture, health, industry, cultural heritage, and human sciences.

The TMIIRR is equipped with four lateral beam tubes (NB1, NB2, NB3, and NB4) to allow the installation of various nuclear facilities around the reactor, such as Prompt Gamma Neutron Activation Analysis (PGNAA), Neutron Imaging (NI), Neutron Diffraction (ND), and so on. The

installation of these facilities requires a preliminary neutron flux characterization, because this will contribute to effectively optimizing the performance and shielding of these facilities.

Prompt Gamma Analysis Activation (PGAA) is a very widely applied technique to simultaneously qualify and quantify the elemental composition of unknown samples, ranging in mass from micrograms to a few grams. This non-destructive technique typically measures in several minutes to several hours per sample. The possibility of detecting a small amount of light elements in a matrix comprised of high-Z elements is another characteristic [1].

Neutron beam characterization is a crucial step before implementing any facility around a nuclear reactor or other neutron source, because it gives a clear idea about the quality of the neutron beam and its suitability for a particular facility or application. Many laboratories around the world characterize their beam facilities and validate them with Monte Carlo models to achieve clear neutron source specifications, either in terms of spectra determination or spatial neutron distribution. For instance, Sandberg et al. [2] used multicomponent activation detectors for measuring neutron energy spectra in the Triga research reactor of Helsinki University of Technology, Finland in 1982. Turkoglu

✉ Hamid Amsil  
amsil@cnesten.org.ma

<sup>1</sup> National Centre for Nuclear Energy, Science and Technology, B.P. 1382, R.P. 10001 Rabat, Morocco

<sup>2</sup> Nuclear Physics Laboratory, Faculty of Science, Mohammed V University, 4 Avenue Ibn Battouta, B.P. 1014, Rabat, Morocco

<sup>3</sup> Unité de Recherche en Physique Et Techniques Nucléaires, Département de Physique, Faculté Des Sciences, Université IbnTofail, B.P. 242, Kenitra, Morocco

et al. [3] characterized a new external neutron beam facility at the Ohio State University using foil activation analysis results and also by simulating a full reactor core model in the MCNP Monte Carlo code. Similarly, the Tehran Research Reactor (TRR) performed the first beam characterization for their NRAD facility in 2016 [4]. For the HRPT Instrument around the Swiss spallation neutron source (SINQ), Talanov et al. [5] validated their MCNP model through the irradiation of detector foils. Viererbl et al. performed as well a neutron beam characterization for the LVR-15 research reactor using detector foils and validated it with an MCNP model. Meanwhile, neutron activation analysis was used by Albarqi et al. [6] to determine the thermal and epithermal neutron flux and its spatial distribution at the beam port of the Missouri University of Science and Technology Research Reactor in 2019. All the above authors reported experimental results showing a good level of agreement with the Monte Carlo models. It is under the frame of these experiences that our work was based. Detector foils were irradiated in the NB1 and NB2 beam tube of the TMIIRR to characterize the neutron flux, and an MCNP6 model was used for validation.

For nuclear analysis techniques such as PGNA, NI, and ND, accurate spectral characteristics for neutrons and neutron flux are important for evaluating the impact on the experiment and the potential accuracy of the methods used. Similar experiments were performed by Tiyaun et al. [7] with an accuracy ranging from 2 to 23% when comparing experimental and calculated results.

Ongoing efforts to characterize neutron beams at the Moroccan TMIIRR for radio isotopes production and neutron activation analysis have been pursued in recent years by Bounouira et al. [8] using detector foils. The most recent attempts comprised detector foil irradiation and measurements. Monte Carlo code was also used to compare with measurement results. The characterization here is concerned with the NB1 and NB2 beam tube, and this forms the subject of this paper.

## Materials and methods

### Triga research reactor description

The TRIGA Mark II reactor is an open pool type research reactor that can be operated at 2 MW maximum power. The core is located near the bottom of an aluminium tank filled with water with 2.5 m in diameter and approximately 8.8 m deep (Fig. 2). Water acts as a moderator and provides adequate protection for the operators standing on top of the reactor. The fuel consists of a mixture of uranium (8.5% wt, enriched at 19.7% in  $^{235}\text{U}$ ), zirconium hydride that provides a moderation effectiveness strongly dependent on fuel

temperature and encapsulated in a stainless steel cladding. The reactor is controlled by five boron carbide control rods while the core consists of 101 fuel elements and 17 graphite elements. To serve the scientific community, TMIIRR is equipped with several irradiation facilities divided into two families in-core and out-core irradiation facilities.

In-core irradiation facilities comprise a pneumatic transfer system (PTS) and a rotary specimen rack (RSR) which are dedicated to neutron activation analysis and the central thimble for radio-isotopes production such as Iodine-131 from the irradiation of  $\text{TeO}_2$  targets.

Out-core irradiation facilities are represented by a Thermal Column (TC) and four beam ports. The TC is a graphite thermal column, 1.2-m by 1.2-m by 1.65-m, extending from the reflector through the concrete structure, provides a source of well thermalized neutrons suitable for physical research or irradiation of biological specimens. A high density concrete mobile door with a removable 20-cm concrete stopper protects the exterior face of this column. The four horizontal beam ports consist of two sections of 15-cm and 20-cm in diameter, extending through the concrete shielding to the face of the reflector, allow for the extraction of core radiation or the insertion of samples for the irradiation. Two (NB3, NB4) of the beam tubes extend radially to the reflector, a third (NB2) penetrates the reflector to the edge of the core and the fourth (NB1) is tangent to the core.

### Experimental device description

The experimental device is conceived to permit the insertion of the threshold monitors at the desired position without any eventual stuck inside the beam tube. This device, designed for the irradiation of flux monitors, is composed of two elements. The first is a plastic support (PS) in the form of a Marinelli beaker, 14-cm in diameter and 10-cm long, with an annular base and a closed top where the vials have been welded to serve as housing for threshold monitors. The welding positions of the vials, numbered from 1 to 9 as shown in Fig. 1, have been chosen so that the measurements will be representative to determine the integrated flux along the cross section of the beam tube. The second element is a PVC tube whose diameter is large enough that slid over the annular part of the PS. This element acts like a holder of the monitor-holder (PS). In order to avoid an eventual disconnection, the PS and the PVC tube, that was sufficiently long to reach the bottom of each beam tube, have been welded. Both the device and the PVC insertion tube were manufactured in house, firstly to ensure that the device fitted with the actual dimensions (diameter and length) of the beam tube and secondly to achieve better accuracy for device positioning.

**Fig. 1** On the right: PS with nine front-sealed PE vials used to contain the activation detector foils; on the left: the experimental assembly for inserting the PS into the beam tube



The high purity PE vials, commonly used in neutron activation analysis, has a cylindrical shape with an outer diameter and height respectively of 9.3-mm and 5.8-mm. Its frontal thickness (cover) is 0.3-mm while the lateral one is 0.65-mm.

Neutron activation experiments were carried out on site using four available high-purity activation detector foils with threshold reactions covering most of the expected neutron spectrum. Table 1 presents the type and specification of each activation detector foil that was used in this experiment.

Eighteen sets of the four labelled activation detectors were prepared, sealed in polyethylene (PE) bags and each packed (set) in the PE vials already welded to the PS.

Activation detectors used in this experiment, manufactured by GoodFellow, are Al-0.1Au, Zn, Ni and Ti. The gold monitor is 1-mm diameter while the others are 0.05-mm, 0.125-mm and 0.125-mm thick respectively for Zn, Ni and Ti (Table 1). All foil activation detectors were prepared as disc shape of about 5-cm diameter while the Al-0.1% Au wire was prepared such that the average weight is about 20-mg. These activation detectors were placed respectively from the bottom of the PE vial in the following order: Ti, Ni, Zn and Au. This order was chosen to minimize the effect of neutrons self-shielding. Nine sets were positioned onto the nine positions of the PS (Fig. 1) to form a single package for one experiment.

### Activation and measurement

The activation of all detector foils was achieved by introducing the whole assembly (see Fig. 2) into the beam tube so that the nine threshold detector sets will be on the plane perpendicular to the channel axes in depth of 310-cm and 353-cm from the beam tube exit respectively for the NB1 and NB2.

Each package of nine detector sets was irradiated for 30 and 60 min under 10 and 50 kW, respectively, within NB1 (A position) and NB2 (B position) (see Fig. 2). The various threshold reactions considered in this experiment are presented in Table 2.

Following irradiation, all individual foil or wire detectors were removed from the nine vials, and they were counted individually using the calibrated high purity germanium detector. The counting time was based upon the induced activity and the half-life of the specific reaction being

measured. This was needed to minimize detector dead-time while also maximizing the total counts and obtaining the best possible statistics.

The reaction rate was calculated by using the activities measured under the photopic corresponding to each monitor. Table 2 illustrates monitors used, reaction types with corresponding isotopes product, half-life of each isotope, gamma radiation energy measured and the reaction threshold. An average activity has been calculated for multigamma isotopes emitters.

### Methods

The gamma lines taken into account during the radioactivity measurements are those due to the reactions  $^{197}\text{Au}(n, g)^{198}\text{Au}$ ,  $^{46}\text{Ti}(n, p)^{46}\text{Sc}$ ,  $^{47}\text{Ti}(n, p)^{47}\text{Sc}$ ,  $^{48}\text{Ti}(n, p)^{48}\text{Sc}$ ,  $^{58}\text{Ni}(n, p)^{58}\text{Co}$ ,  $^{64}\text{Zn}(n, g)^{65}\text{Zn}$  and  $^{68}\text{Zn}(n, g)^{69}\text{Zn}$  whose values are presented in the Table 2. All Monte Carlo calculations were performed through the transport Monte Carlo MCNP6 2.6.0 [9] code and the ENDF 7.1 V2013 data libraries.

An approximated MCNP6 model for the TMIIR was created. This model (see Fig. 3) included the reactor core, thermal column and biological shielding, with it containing 101 fuel rods and 17 graphite bars, a graphite reflector, a light water moderator, and the four horizontal beam tubes. The MCNP6 input was prepared in such a way that a very quick setup of any desired core configuration. The MCNP6 calculations were run with 3,000,000,000 active histories. A total of 3,000,000 histories per cycle were used and 1,010 cycle of neutrons. The initial effective multiplication factor ( $k_{\text{eff}}$ ) value was chosen to be 1.04069 and the first 10 cycles were skipped to obtain a well-distributed neutron source. To account for thermal neutron scattering, the appropriate  $s(\alpha, \beta)$  treatment was applied to graphite, zirconium hydride

**Table 1** Flux monitors used in the experiment and their specifications

Detector type	Shape	Thickness/diameter (mm)	Purity (%)
Au	Wire	1	0.1
Ni	Foil	0.125	99.95
Ti	Foil	0.125	99.99+
Zn	Foil	0.05	99.99+

**Fig. 2** Top view of the TMRI-IRR and the irradiation positions (A position in NB1 and B position in NB2)

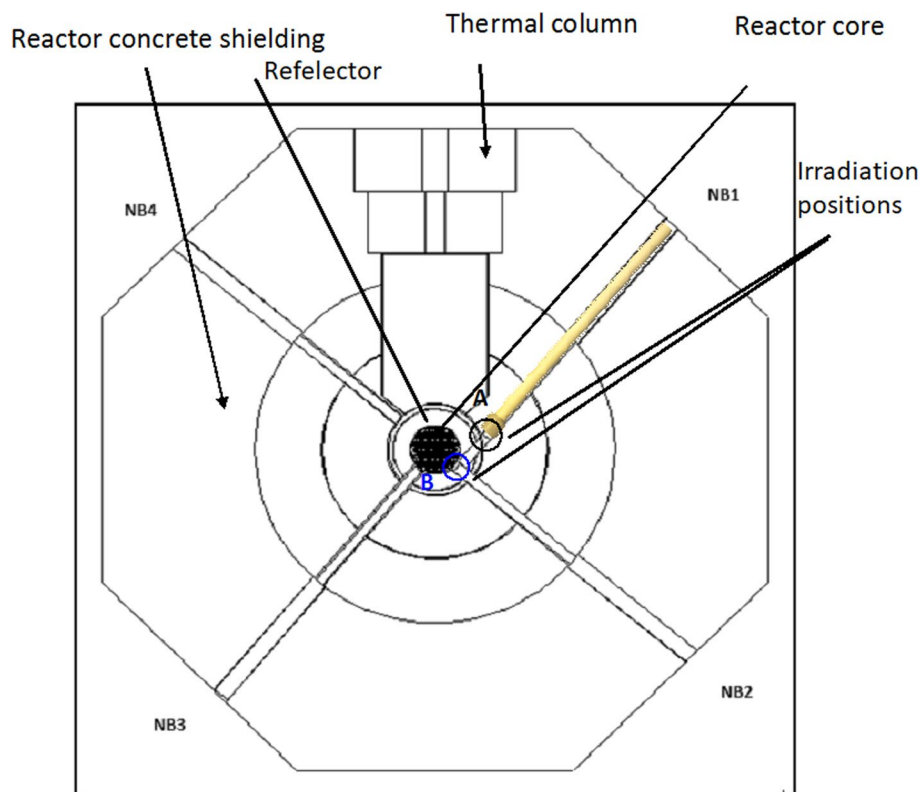


**Table 2** Threshold reactions used in this experiment

Detector	Reaction	Half-life	Gamma energy (keV)	Intensity (%)	Threshold neutron energy MeV
Gold	$^{197}\text{Au}(n, \gamma)^{198}\text{Au}$	2.69 d	411.8	95.6	–
Nickel	$^{58}\text{Ni}(n, p)^{58}\text{Co}$	70.88 d	810.8	99.4	0.812
Titanium	$^{46}\text{Ti}(n, p)^{46}\text{Sc}$	83.83 d	889.3; 1120.5	99.9; 99.9	1.619
Titanium	$^{47}\text{Ti}(n, p)^{47}\text{Sc}$	3.35 d	159.4	68.3	0.0749
Titanium	$^{48}\text{Ti}(n, p)^{48}\text{Sc}$	1.82 d	983.5; 1312.1; 1 037.5	99.9; 99.9; 97.6	3.274
Zinc	$^{64}\text{Zn}(n, \gamma)^{65}\text{Zn}$	244.26 d	1 115.5	50.22	–
Zinc	$^{68}\text{Zn}(n, \gamma)^{69\text{m}}\text{Zn}$	13.76 h	438.6	94.77	–

and water to simulate the low-energy neutron interactions. The model was subjected to test the KCODE criticality mode with fresh fuel loaded in the reactor core. The  $k_{\text{eff}}$  was then obtained to be  $1.04160 \pm 0.00001$ .

The experimental device was modelled in such a way that the comparison between the results of measurements and those of the simulation will be as representative as possible. The MCNP6 model of the PE vials was denoted by five areas limited by the intersection of several planes and cylinders. These four areas are the cover which measures 0.3-mm, the base measuring 0.3-mm, the side with a thickness of 0.650-mm and the interior of the vial which will house the flux monitors. The monitors were represented, in the form of discs, by the intersection of cylinders of 5-cm in diameter

and parallel planes with the exception of gold which has a different shape (wire). The latter was represented in cylindrical form positioned horizontally in the medium of the area between the bottom of the vial cover and the top surface of the Zn monitor (see Fig. 4). The distances between the planes represent the thicknesses of the foil monitors. This has been applied for all nine monitors. All the foil flux monitors have been placed, stuck to each other, in the bottom of the vial. The PS and the PVC tube were not taken into consideration in this MCNP6 model.

The F2 tally was used to determine the flux at the surfaces limiting the threshold detectors. In order for the comparison between the experimental and calculated results to be accurate, we calculated the neutron flux at approximately

**Fig. 3** MCNP6 model of the TMRIIRR with calculation positions and particle source distribution including the PE vials at NB1 beam tube

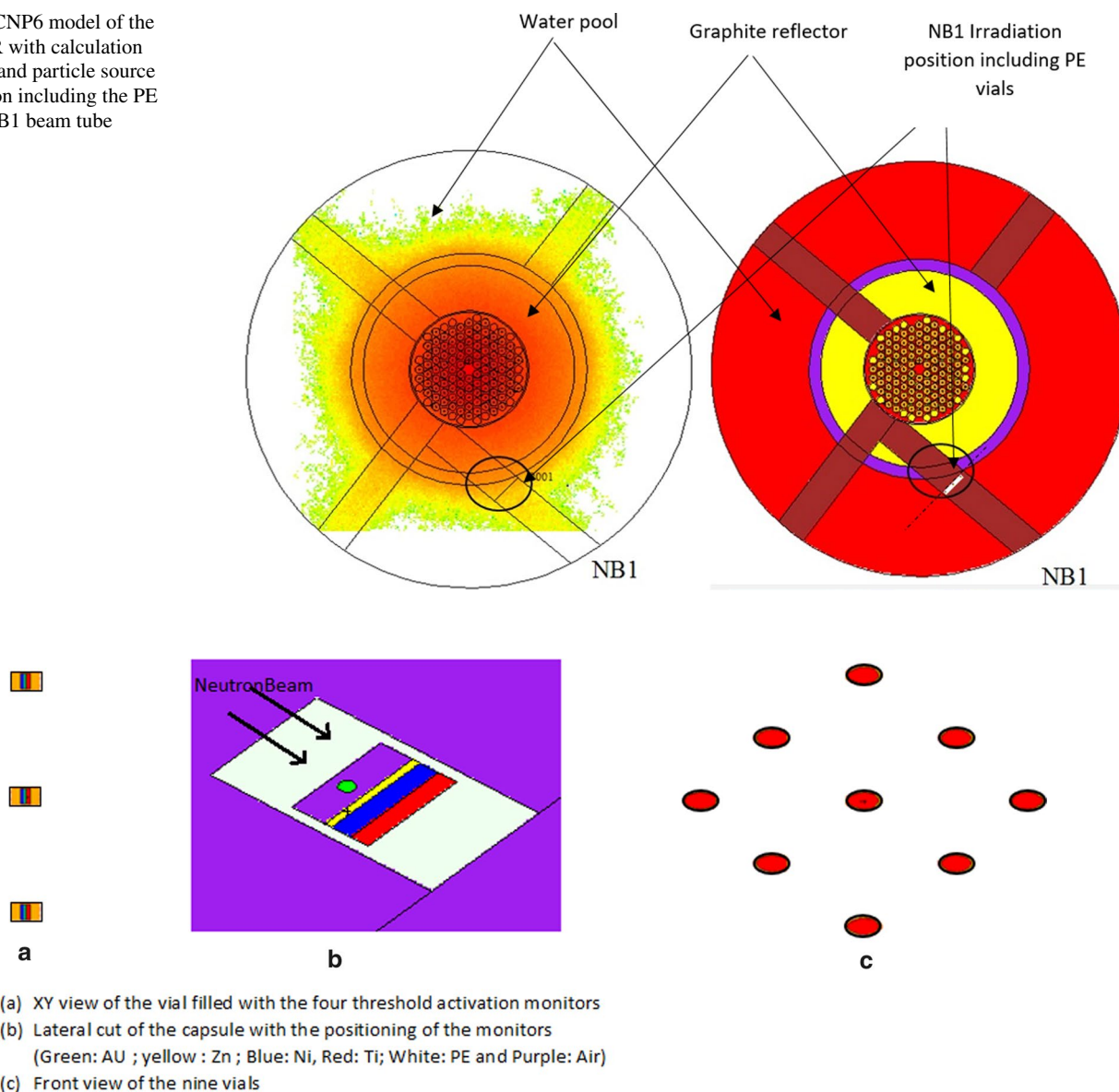


**Fig. 4** MCNP6 model of the PE vials with the associated threshold monitors (scale is not respected)

the same positions as in the experiment (see Fig. 3), and the flux was also bin averaged to the energy groups (0.0, 0.4 eV), (0.4 eV, 10 keV), and (10 keV, 20 meV) for the nine PS positions for comparison with the experimental results.

## Results and discussion

The isotope's total activity was calculated as the area under the associated gamma peak and calculated using a non-linear least-squares algorithm provided by the detector software in order to remove background effects. The measured activity was then extrapolated to saturation. The

neutron flux averages were calculated using measurement and MCNP6 code for the NB1 and NB2 beam tube. Once irradiation-induced activity was measured, the neutron flux was determined consequently based on the reaction rate which are presented in Table 3. The measured averaged values of thermal (0.0, 0.4 eV), epithermal (0.4 eV, 10 keV), and fast (10 keV, 20 meV) neutron fluxes for both beam tubes, under respectively 10-KW and 50-KW operational core power, linearly extrapolated to 2 MW, are presented with the calculated ones for comparison.

The neutron flux results obtained for the nine positions using the measurement and MCNP6 code are shown in



**Table 3** Reaction rates associated to each reaction used for measurements

Position	$^{197}\text{Au}(n, g)^{198}\text{Au}$	$^{46}\text{Ti}(n, p)^{46}\text{Sc}$	$^{47}\text{Ti}(n, p)^{47}\text{Sc}$	$^{48}\text{Ti}(n, p)^{48}\text{Sc}$	$^{58}\text{Ni}(n, p)^{58}\text{Co}$	$^{64}\text{Zn}(n, g)^{65}\text{Zn}$	$^{68}\text{Zn}(n, g)^{69}\text{Zn}$
<i>RR (s<sup>-1</sup>) NB1</i>							
1	7.78E-12	1.17E-16	2.41 E-16	3.66 E-18	2.68 E-16	4.13 E-14	4.51 E-15
2	7.77 E-12	1.37 E-16	2.43 E-16	3.59 E-18	2.90 E-16	4.40 E-14	4.51 E-15
3	7.98 E-12	1.35 E-16	2.72 E-16	4.11 E-18	4.02 E-16	4.15 E-14	4.59 E-15
4	5.90 E-12	1.20 E-16	2.04 E-16	3.04 E-18	3.65 E-16	4.80 E-14	4.63 E-15
5	5.53 E-12	1.27 E-16	2.07 E-16	3.09 E-18	3.32 E-16	4.47 E-14	4.36 E-15
6	5.35 E-12	1.38 E-16	2.16 E-16	3.37 E-18	3.43 E-16	3.88 E-14	4.38 E-15
7	5.33 E-12	1.20 E-16	2.01 E-16	2.98 E-18	3.51 E-16	4.12 E-14	4.35 E-15
8	5.45 E-12	1.12 E-16	1.97 E-16	3.03 E-18	3.07 E-16	3.68 E-14	4.48 E-15
9	5.36 E-12	1.22 E-16	2.18 E-16	3.66 E-18	3.93 E-16	4.58 E-14	4.35 E-15
Average	6.27 E-12	1.25 E-16	2.22 E-16	3.39 E-18	3.39 E-16	4.25 E-14	4.46 E-15
RSD	19.01%	7.50%	11.27%	11.50%	13.37%	8.27%	2.40%
<i>RR (s<sup>-1</sup>) NB2</i>							
1	4.59 E-11	3.46 E-16	7.15 E-16	1.08 E-17	5.37 E-15	2.56 E-13	1.23 E-14
2	4.75 E-11	4.16 E-16	7.38 E-16	1.09 E-17	5.89 E-15	2.30 E-13	2.45 E-14
3	4.49 E-11	3.45 E-16	6.98 E-16	1.05 E-17	5.01 E-15	2.39 E-13	2.42 E-14
4	4.92 E-11	4.17 E-16	7.06 E-16	1.05 E-17	5.16 E-15	2.57 E-13	1.27 E-14
5	4.53 E-11	4.75 E-16	7.77 E-16	1.16 E-17	6.31 E-15	2.15 E-13	2.35 E-14
6	4.76 E-11	5.08 E-16	7.93 E-16	1.24 E-17	3.33 E-15	2.53 E-13	1.24 E-14
7	4.38 E-11	4.60 E-16	7.74 E-16	1.14 E-17	5.45 E-15	2.24 E-13	2.29 E-14
8	4.67 E-11	4.39 E-16	7.69 E-16	1.18 E-17	5.66 E-15	2.51 E-13	1.21 E-14
9	4.59 E-11	4.50 E-16	8.00 E-16	1.35 E-17	6.38 E-15	2.14 E-13	1.03 E-15
Average	4.63 E-11	4.29 E-16	7.52 E-16	1.15 E-17	5.40 E-15	2.38 E-13	1.62 E-14
RSD	3.54%	12.78%	5.14%	8.36%	16.82%	7.36%	49.83%

Tables 4 and 5 for NB1 and NB2 respectively. A relative standard deviation (RSD<sup>1</sup>) of around 17.93% and 10.27% is observed respectively for the measured and calculated values of the average total flux at the level of the NB1 beam tube. With regards to the NB2 beam tube, 8.84% and 4.44% are the RSDs calculated respectively for the results obtained by measurement and MCNP6 code.

The average total neutron flux for the NB1 beam tube, as shown in Table 4, show a relatively good agreement between the measured and calculated results with 37.53% difference. Neutron flux components for the NB1 beam tube, show a concordance between the calculated and measured results with a maximum difference of 27.53% which corresponds to the average neutron flux related to the energy group (0.4 eV, 10 keV). Figure 5 illustrates the distribution of the neutron flux in the studied positions obtained for the measured and calculated values in the NB1 beam tube for the total and the three energy groups of the neutron flux. A fall in the neutron flux measured in the NB1 beam tube is observed between the position numbers 1, 2, 3 and 4, 5, 6, 7, 8, 9 for the three energy groups, which does also appear in the

calculations obtained by the code MCNP6. The maximum of this drop is around 41.56% corresponding to the energy group (0.0, 0.4 eV) between the positions 3 and 4 of the measured results.

The total average neutron flux again shows a good level of agreement between the measured and calculated values for the NB2 beam tube with 20.01% difference (Table 5). The investigation related separately to the total and the three components of the flux shows that the curves keep relatively the same shape for both the measured and calculated values (Fig. 6). The corresponding RSDs are 27.87%, 26.67% and 22.82% related respectively to (0.0, 0.4 eV), (0.4 eV, 10 keV), and (10 keV, 20 meV) energy ranges. It can be noticed that the positions (5, 6, 7, 8 and 9) closest to the axis of the beam represent a good agreement between measurements and calculations with respect to the others.

Knowing that the real flux present in the beam tube has undergone thermalization as well as a possible backscattering of neutrons because of the experimental device, a comparison of the fluxes with and without the PE vials was carried out by calculation. The correction factors were determined for the three groups of energies in order to have significant flux values. The results show a decrease of 7.30% and 14.81% and 19.31% respectively for the thermal, epithermal and fast neutron flux.

<sup>1</sup> RSD = (Standard deviation/Average) \* 100%

**Table 4** Measured and calculated neutron flux at the NB1 beam tube for the nine positions for the three energy groups including the total flux

Position number	Measurement		MCNP6		(Meas.- Cacl.)/Meas. (%)
	Measurement	Err. (%)	Calculation	Err. (%)	
<i>Average total neutron flux NBI</i>					
1	3.46E+12	6.20E+11	4.50E+12	9.58E+11	30.26
2	3.46E+12	6.20E+11	4.33E+12	6.15E+11	24.97
3	3.60E+12	6.45E+11	3.36E+12	6.18E+11	6.77
4	2.69E+12	4.82E+11	3.53E+12	5.37E+11	31.36
5	2.51E+12	4.51E+11	4.11E+12	4.80E+11	63.28
6	2.44E+12	4.38E+11	3.43E+12	5.42E+11	40.43
7	2.44E+12	4.37E+11	3.80E+12	6.34E+11	56.00
8	2.47E+12	4.43E+11	4.03E+12	5.44E+11	63.20
9	2.47E+12	4.42E+11	4.03E+12	6.54E+11	63.63
Average	2.84E+12		3.90E+12		37.53
RSD (%)	17.93%		10.27%		
<i>Average thermal neutron flux NBI (0.0 eV, 0.4 eV)</i>					
1	2.22E+12	3.33E+11	2.83E+12	1.01E+12	27.44
2	2.22E+12	3.33E+11	2.43E+12	3.27E+11	9.75
3	2.28E+12	3.42E+11	1.90E+12	1.19E+11	16.76
4	1.68E+12	2.53E+11	1.96E+12	2.03E+11	16.13
5	1.58E+12	2.37E+11	2.35E+12	2.61E+11	49.11
6	1.53E+12	2.29E+11	1.95E+12	1.54E+11	27.62
7	1.52E+12	2.28E+11	2.15E+12	1.94E+11	41.14
8	1.56E+12	2.33E+11	2.30E+12	2.24E+11	48.10
9	1.53E+12	2.29E+11	2.30E+12	1.77E+11	50.50
Average	1.79E+12	2.69E+11	2.24E+12	2.96E+11	25.19
RSD	19.01%		13.17%		
<i>Average epithermal neutron flux NBI (0.4 eV, 10 keV)</i>					
1	7.38E+11	1.11E+11	5.44E+11	1.94E+11	26.24
2	7.36E+11	1.10E+11	4.68E+11	6.28E+10	36.46
3	7.57E+11	1.14E+11	3.65E+11	2.29E+10	51.80
4	5.60E+11	8.39E+10	3.76E+11	3.91E+10	32.77
5	5.24E+11	7.86E+10	4.53E+11	5.02E+10	13.68
6	5.07E+11	7.61E+10	3.75E+11	2.96E+10	26.13
7	5.05E+11	7.58E+10	4.13E+11	3.72E+10	18.31
8	5.17E+11	7.75E+10	4.43E+11	4.31E+10	14.25
9	5.08E+11	7.62E+10	4.42E+11	3.40E+10	12.87
Average	5.95E+11		4.31E+11		27.53
RSD (%)	19.01%		13.17%		
<i>Average fast neutron flux NBI (10 keV, 17 MeV)</i>					
1	4.99E+11	7.49E+10	6.67E+11	9.16E+10	33.51
2	5.08E+11	7.62E+10	6.23E+11	1.97E+11	22.64
3	5.65E+11	8.47E+10	5.01E+11	1.55E+11	11.32
4	4.45E+11	6.67E+10	5.34E+11	1.66E+11	20.16
5	4.13E+11	6.19E+10	5.99E+11	1.34E+11	45.08
6	4.08E+11	6.12E+10	4.94E+11	1.43E+11	21.09
7	4.10E+11	6.15E+10	5.72E+11	1.70E+11	39.57
8	3.99E+11	5.98E+10	5.80E+11	1.50E+11	45.47
9	4.29E+11	6.43E+10	5.79E+11	1.69E+11	35.13
Average	4.53E+11	6.79E+10	5.72E+11	1.53E+11	26.36
RSD (%)	12.77%		9.76%		

**Table 5** Measured and calculated neutron flux at the NB2 beam tube for the nine positions for the three energy groups including the total flux

Position	Measurement		MCNP6		(Meas.- Cacl.)/Meas. (%)
	Measurement	Err. (%)	Calculation	Err. (%)	
<i>Average total neutron flux NB2</i>					
1	1.18E+13	1.77E+12	9.20E+12	1.07E+12	21.93
2	1.40E+13	2.09E+12	9.74E+12	1.11E+12	30.21
3	1.05E+13	1.58E+12	9.50E+12	1.05E+12	9.69
4	1.29E+13	1.93E+12	1.03E+13	1.15E+12	19.66
5	1.12E+13	1.68E+12	9.40E+12	1.07E+12	16.16
6	1.26E+13	1.88E+12	9.87E+12	1.12E+12	21.33
7	1.09E+13	1.64E+12	8.85E+12	1.04E+12	18.96
8	1.20E+13	1.80E+12	9.53E+12	1.10E+12	20.77
9	1.19E+13	1.78E+12	9.72E+12	1.08E+12	18.07
Average	1.20E+13		9.57E+12		20.01
RSD (%)	8.84%		4.44%		
<i>Average thermal neutron flux NB2 (0.0 eV, 0.4 eV)</i>					
1	5.61E+12	8.41E+11	7.47E+12	7.47E+11	33.19
2	6.50E+12	9.75E+11	7.20E+12	7.20E+11	10.83
3	5.40E+12	8.10E+11	6.98E+12	6.98E+11	29.18
4	5.88E+12	8.83E+11	7.37E+12	7.37E+11	25.29
5	5.36E+12	8.04E+11	6.92E+12	6.92E+11	29.21
6	6.05E+12	9.07E+11	7.99E+12	7.99E+11	32.13
7	5.50E+12	8.25E+11	7.29E+12	7.29E+11	32.51
8	6.13E+12	9.20E+11	7.72E+12	7.72E+11	25.89
9	5.51E+12	8.27E+11	7.48E+12	7.48E+11	35.64
Average	5.77E+12	5.85E+10	7.38E+12	7.85E+11	27.87
RSD (%)	6.76%		4.58%		
<i>Average epithermal neutron flux NB2 (0.4 eV, 10 keV)</i>					
1	2.58E+12	5.17E+11	1.78E+12	2.68E+11	30.93
2	3.13E+12	6.25E+11	1.95E+12	2.93E+11	37.59
3	2.22E+12	4.44E+11	1.84E+12	2.77E+11	16.87
4	2.90E+12	5.81E+11	2.28E+12	3.41E+11	21.58
5	2.49E+12	4.99E+11	1.85E+12	2.78E+11	25.73
6	2.83E+12	5.66E+11	2.02E+12	3.04E+11	28.45
7	2.38E+12	4.76E+11	2.07E+12	3.10E+11	13.09
8	2.63E+12	5.26E+11	1.96E+12	2.94E+11	25.43
9	2.69E+12	5.38E+11	1.73E+12	2.59E+11	35.69
Average	2.65E+12	5.53E+10	1.94E+12		26.67
RSD (%)	10.44%		8.60%		
<i>Average fast neutron flux NB2 (10 keV, 17 MeV)</i>					
1	3.59E+12	7.18E+11	2.44E+12	2.44E+11	31.94
2	4.34E+12	8.68E+11	2.98E+12	2.98E+11	31.26
3	2.90E+12	5.80E+11	2.60E+12	2.60E+11	10.49
4	4.09E+12	8.18E+11	2.76E+12	2.76E+11	32.44
5	3.36E+12	6.72E+11	2.87E+12	2.87E+11	14.63
6	3.68E+12	7.35E+11	2.61E+12	2.61E+11	28.88
7	3.03E+12	6.07E+11	2.82E+12	2.82E+11	6.98
8	3.27E+12	6.53E+11	2.73E+12	2.73E+11	16.50
9	3.65E+12	7.31E+11	2.81E+12	2.81E+11	23.04
Average	3.55E+12	7.09E+11	2.74E+12	2.74E+11	22.82
RSD (%)	13.18%		5.95%		



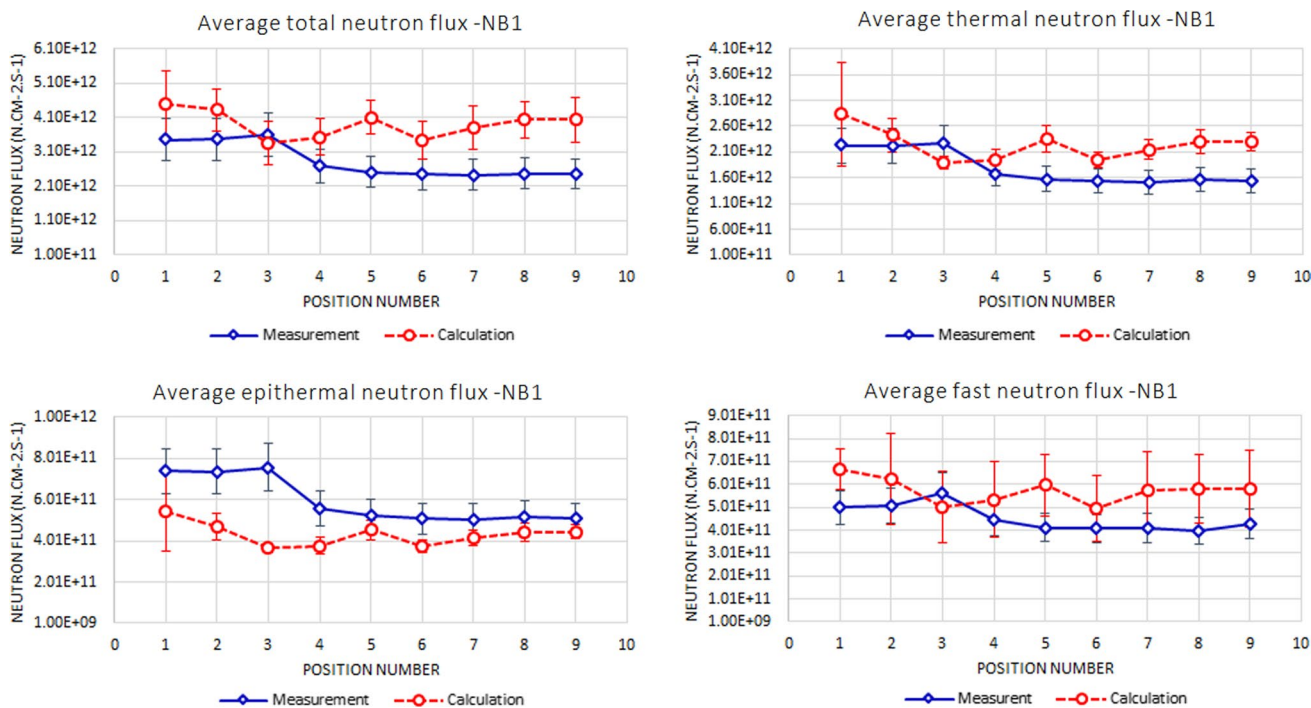


**Fig. 5** Neutron flux distribution in the nine studied positions obtained for the measured and calculated values in the NB1 beam tube for the three energy groups

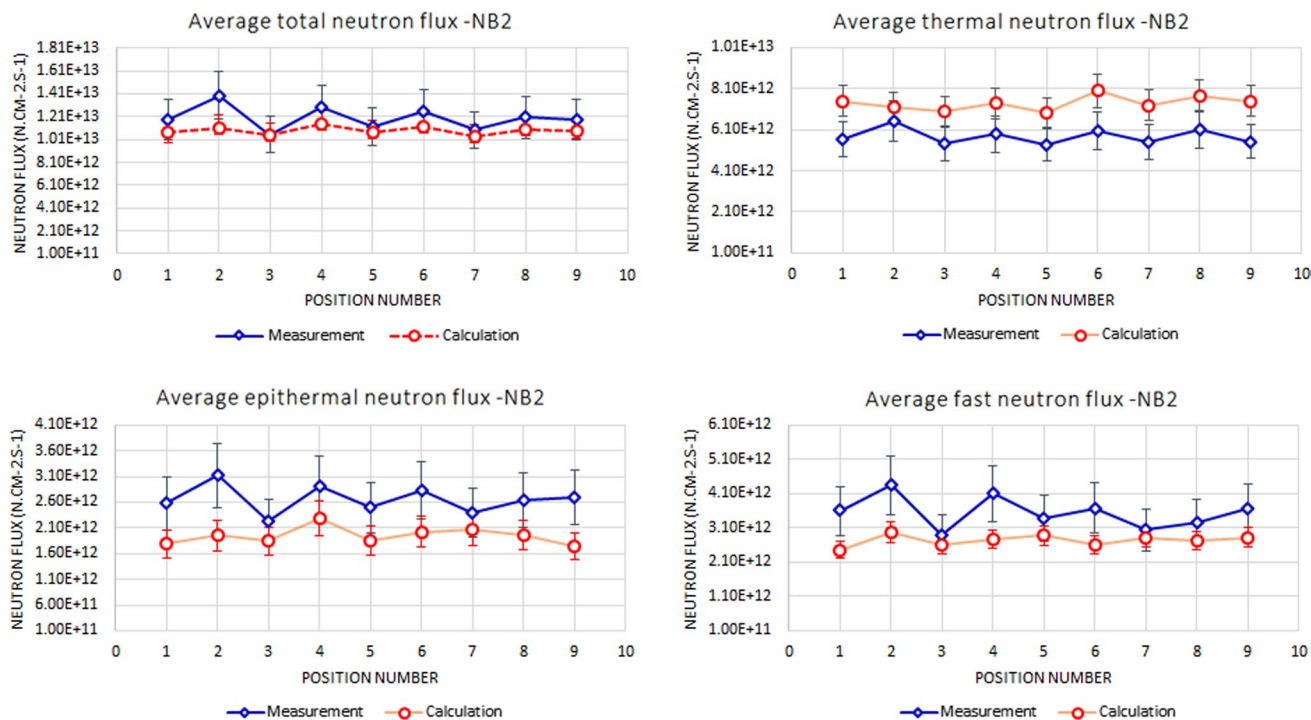


**Fig. 6** Neutron flux distribution in the nine studied positions obtained for the measured and calculated values in the NB2 beam tube for the three energy groups

## Conclusions

This preliminary neutron flux characterization for the NB1 and NB2 beam tube was performed successfully using threshold activation detectors and MCNP6 code calculations. The results are considered preliminary, but they can be used as input for setting up the PGNAA/NI and ND around the NB1 and NB2 beam tube respectively.

On the other hand, as a future investigation, the flux evaluation and validation warrant further investigation that may involve more threshold activation detector at a sufficiently high power to obtain good measurement accuracy and a more precise MCNP6 model for the TMIIRR.

**Acknowledgements** This work was conducted under the framework of the MOR1009 project, which is supported by the International Atomic Energy Agency.

## References

1. Amsil H, Jalil A, Embarch K, Bounouira H et al (2020) Conceptual implementation stages for Moroccan PGAA/NI instruments: STAGE I & II. *J Neutron Res* 22:403–415
2. Sandberg JV, Lund PD (1983) Determination of reactor neutron spectra with multicomponent activation detectors. *J Radioanal Chem* 76:151–170
3. Turkoglu D, Burke J, Lewandowski R et al (2012) Characterization of a new external neutron beam facility at the Ohio State University. *J Radioanal Chem* 291:321–327
4. Choopan Dastjerdi MH, Khalafi H, Kasesaz Y, Mirvakili SM, Emami J, Ghods H, Ezzati A (2016) Design, construction and characterization of a new neutron beam for neutron radiography at the Tehran Research Reactor, NASA Astrophysics Data System (ADS), 2016-05-01
5. Talanov V, Cheptiakov D, Filges U, Forss SH, Panzner T, Pomjakushin V, Rantsiou E (2014) Thermal neutron beam characterization at the HRPT instrument at the Swiss spallation neutron source. In: WEPRO077 proceedings of IPAC 2014, Dresden, Germany
6. Albarqi M, Alsulami R, Akyurek T, Graham J (2019) Neutron flux characterization of the beam port of the Missouri University of Science and Technology Reactor. *J Radioanal Chem* 321:109–116
7. Tiyaun K, Chintin M, Munsorn S, Somchit S (2015) Validation of the MCNP computational model for neutron flux distribution with the neutron activation analysis measurement. *J Phys Conf Ser* 611:012007
8. Bounouira H, Embarch K, Bounakhla M (2014) Neutron flux characterization of the Moroccan Triga Mark II research reactor and validation of the k0 standardization method of NAA using k0-IAA program. *J Radioanal Nucl Chem* 300:465–471
9. MCNP (2003) A general Monte Carlo N-particle transport code, version 5 (Revised 10/3/05)

**Publisher's Note** Springer Nature remains neutral with regard to jurisdictional claims in published maps and institutional affiliations.